Pergamon

Int. J. Heat Mass Transfer. Vol. 40, No. 11, pp. 2621–2636, 1997

Printed in Great Britain
0017-9310/97 $17.00+0.00

PII: S0017-9310(96)00281-5

Onset of thermally induced gas convection in mine wastes

NING LU
U.S. Geological Survey, Lakewood, CO 80225, U.S.A.

and

YIQIANG ZHANG
S.S. Papadopulos and Associates, Inc., Bethesda, MD 20814, U.S.A.

(*Received* 29 *May* 1996 *and in final form* 5 *August* 1996)

Abstract—A mine waste dump in which active oxidation of pyritic materials occurs can generate a large amount of heat to form convection cells. We analyze the onset of thermal convection in a two-dimensional, infinite horizontal layer of waste rock filled with moist gas, with the top surface of the waste dump open to the atmosphere and the bedrock beneath the waste dump forming a horizontal and impermeable boundary. Our analysis shows that the thermal regime of a waste rock system depends heavily on the atmospheric temperature, the strength of the heat source and the vapor pressure.

INTRODUCTION

Acid mine drainage is an environmental pollution problem caused by the release of sulfuric acid from mine wastes and abandoned mines into surface or ground water. Sulfuric acid and hydrogen ions are generated by the oxidation of pyrite and other sulfide minerals which commonly exist in coal and metal mining wastes. Oxidation is an exothermic process that produces a large amount of heat. Fielder [1] found that 90 kJ of heat is released for each mole of pyrite. If the heat capacity of mining wastes is 568 J kg^{-1}, this amount of heat is enough to raise the temperature of a kilogram of waste rock by about 1.6° K, or is enough to vaporize 0.7 g of water. Therefore, the heating within a waste rock dump undergoing active oxidation can be very large. Field measurements [2, 3] show that the temperature can be as much as 63 K warmer than the atmosphere in waste rock piles with heights of 20–30 m.

Extensive work has been done in studying the controls on the acid generation process. The major controls include oxygen transport, chemical-kinetic and biochemical controls on oxidation rates, heat source strength and ground-water flow. Modeling studies [4, 5] have shown that the geometry of the dump also has an important effect on the rate of oxidation because larger topographic relief on the dump sides tends to promote air flow into the dump base and upward circulation, enhancing oxidation rates. Figure 1 shows acid mine drainage in a waste rock dump conceptually. The volume of a waste rock dump can be as large as tens of millions of cubic meters, making its size several kilometres in width and tens of meters in depth. Because waste rock dumps stand above the surrounding ground surface, all or part of the dump may be unsaturated. The typical shape of a waste dump is a flat surface with sloped sides as depicted in Fig. 1. Waste rock from coal and some metal mining usually contains a high concentration of pyritic materials. Some waste contains as much as 7% of pyritic materials [3]. Due to the nature of mining activities, waste rock usually is very loose and has high porosity. Therefore, oxygen in the surrounding environment can easily diffuse or flow into the dump. Under ordinary temperature conditions (274–373 K), oxidation will take place and sulfuric acid, hydrogen ions and heat will be released. Because acid generation is an exothermic chemical reaction process, a feedback mechanism exists between heat production and gas flow [6] so that heating provides a driving force for gas flow [7] and gas flow, in turn, enhances the supply of oxygen.

Another factor which complicates the oxidation process is the presence of bacteria. Temple and Koehler [8] and Lorenz and Tarpley [9] demonstrated that bacteria catalyze the oxidation reaction. Certain species of bacteria was found to increase the rate of oxidation by two orders of magnitude. On the other hand, bacterial oxidation seems to stop when the temperature exceeds 330 K [10]. At present, the upper limit of the temperature that may be reached due to the oxidation reaction is not known. Temperatures as high as 353 K have been observed in dumps of low-

NOMENCLATURE

A_0	dimensionless coefficient
B_0	dimensionless coefficient
c_1^0	integral coefficient
c_2^0	integral coefficient
c_p^{gas}	specific heat of gas [J kg^{-1} K^{-1}]
c_p^{rock}	specific heat of rock [J kg^{-1} K^{-1}]
C_0	ambient oxygen concentration, 9.4 [mol m^{-3}]
D_e	oxygen diffusion coefficient [m^2 s^{-1}]
D_0	time constant parameter
E_0	dimensionless coefficient
f	function defined in equation (A-11)
F	heat production constant [J mol^{-1}]
F_0	dimensionless coefficient
g	gravitational acceleration [m s^{-2}]
H	thickness of layer [m]
H_v	heat of vaporization of water [J kg^{-1}]
k	intrinsic permeability of rock [m^2]
K_t	thermal conductivity of rock [J K^{-1} m^{-1} s^{-1}]
l	horizontal wave number
m	vertical wave number
n	porosity [dimensionless]
P	gas pressure [kg m^{-1} s^{-2}]
P_a	defined by $P_a = P - P_v$ [kg m^{-1} s^{-2}]
P_v	vapor pressure of water [kg m^{-1} s^{-2}]
$\mathbf{q}$	gas flux [m^3 s^{-1}]
R	gas constant [kg m^2 s^{-2} mol^{-1} K^{-1}]
R_a	Rayleigh number
S_0	heat source intensity constant [J m^{-3} s^{-1}]
S_h	internal heat source [J m^{-3} s^{-1}]
t	time [s]
T	absolute temperature [K]
ΔT	temperature difference between lower and top boundaries [K]
$\hat{W}$	solution function of vertical flux
$\bar{w}$	dimensionless vertical flux
x	horizontal coordinate [m]
z	vertical coordinate [m]
$\mathbf{z}$	downward pointing unit vector.

Greek symbols

α	defined by $g\Omega_a H/R\Delta T$
γ	time rat constant [s^{-1}]
Γ_b	temperature gradient at $z = 1$
δ	Kronecker delta
ζ	dimensionless vertical coordinate
Θ	coefficient of temperature solution
θ	dimensionless temperature
λ	heat source decay constant
λ_1	defined in equation (19)
λ_2	defined in equation (19)
μ	viscosity of gas [kg m^{-1} s^{-1}]
Π	defined in equation (A-16)
ρ	density of gas [kg m^{-3}]
ρ_{rock}	density of rock [kh m^{-3}]
Φ	stream function
Ω_a	molar weight of dry air [kg mol^{-1}]
Ω_v	molar weight of water [kg mol^{-1}].

Subscripts

0	static solution
b	quantity at bottom where $z = 1$
s	quantity at surface where $z = 0$
j,k	rank or summation indices
1,2	mode indices.

Superscripts

$'$	fluctuating quantity
$\bar{}$	dimensionless quantity
*	instability threshold
†	second instability threshold
	trial solution.

grade copper in Bulgaria [2]. A modeling study by Pantelis and Ritchie [11] predicted that the temperature inside a waste dump can reach as high as 373 K. During the acid generation process, the oxygen supply is believed to play an important role. The form of oxygen transport was first identified as diffusion within waste rock [12–15]. Since then, diffusion has been widely presumed as the dominant transport mode [16]. Recent models [4, 5, 11, 17] have considered thermal convection as an additional means of oxygen transport. It is widely accepted that thermal convection can be important only when air permeabilities in the waste rock are high. Based on a study of air transport mechanisms, Bennett *et al.* [4] concluded that convection can occur only when the air permeability of the waste is greater than 10^{-10} m^2, which corresponds to the permeability of gravel and clean sands.

Thermal convection in fluids heated from below is a classical problem and has been studied extensively in both pure fluids and porous media. Studies [18–22] on the onset of thermal convection in both pure fluid and fluid in porous media show that heat transfer and fluid flow combine to form a complicated, coupled process. Whether convective flow will occur depends in a dimensionless number, called the "Rayleigh number." In unsaturated porous media, the Rayleigh number is generally defined by parameters such as air permeability, thermal conductivity, and thickness of the porous layer. Thermal convection of gases in unsaturated porous media has not been extensively studied from the prospective of the onset of con-

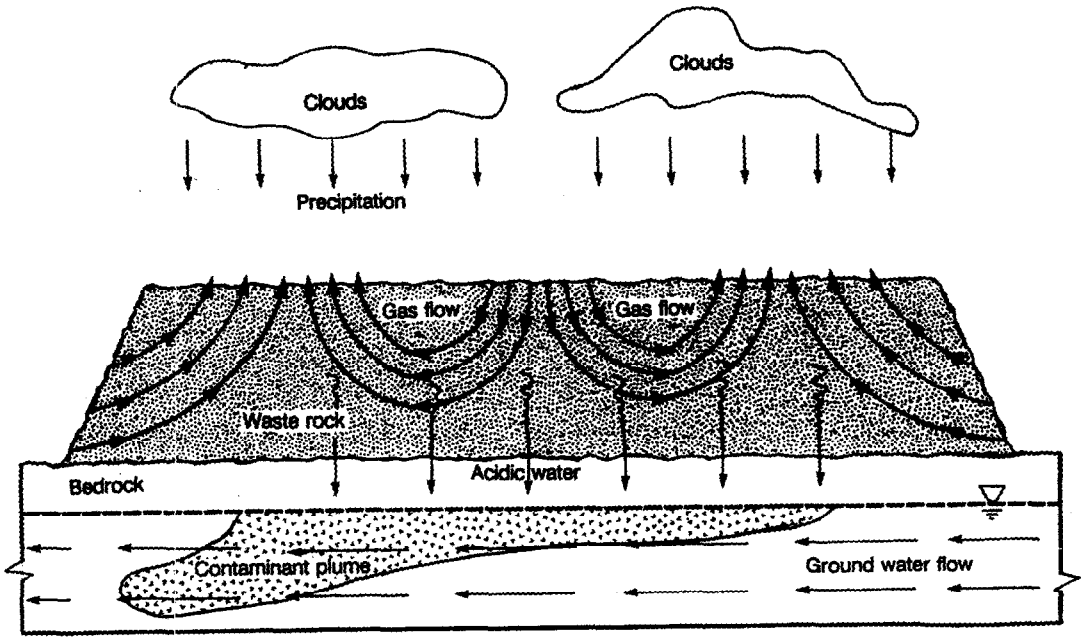

Fig. 1. A conceptual model of acid mine drainage process in waste rock.

vection cells. Only recently has it begun to draw the attention of some researchers. Because the governing equations for unsaturated gas flow and heat transfer are highly nonlinear, it is a difficult and challenging problem. Plumb [23] discussed the modeling of convection in unsaturated porous media with and without boiling or condensation. The drying of porous media has been surveyed by Plumb [23] and Bories [24]. These studies emphasized the thermal regime near or above the boiling point of water. Tien and Vafai [25] and Nield and Bejan [26] provide general reviews of convection in unsaturated porous media. Saathjian [27] and Nield [20] extended previously derived solutions for the onset of thermal convection to a porous medium containing a dry ideal gas. Tsang and Pruess [28] studied thermal convection near a high-level nuclear waste repository in a partially saturated porous medium. Recently, Zhang *et al.* [29] studied the onset of thermal convection in moist, unsaturated porous media.

The fundamental question we attempt to stress here is the conditions under which thermal convection will be important to heat and mass transfer in waste rock dumps. Powers *et al.* [30] study the onset condition for gas flow in snow and conclude that latent heat is very important for phase change between water vapor and ice. The fact that the latent heat is very important to convection in snow suggests that the convective heat transfer could be significant in mine waste because mine waste dumps are generally under much warmer and moist conditions. Numerical studies by Ross *et al.* [31] show that convection may play an important role for heat transfer in large, moist, unsaturated porous systems.

Generally, flow and heat transfer in waste rock are strongly coupled. Heat and mass transfer can be in three distinct regimes: conduction dominated where oxygen is mainly supplied by diffusion, stable convection and chaotic. The transitions between these regimes can be found by stability analysis of the governing equations. The Rayleigh number controls the heat and flow regime. We will discuss the onset process in more details later in the Analysis section. We employ a perturbation technique to solve the stability problem. The perturbation technique, which is the usual method of solving convective instability problems [32, 33], involves three steps. First, the governing equations are solved assuming no convective flow to give the so-called static solution. Second, the static solution is perturbed slightly in as general a manner as possible consistent with the boundary conditions. At this step, appropriate dimensionless quantities are identified and the perturbation equations are reformulated as an eigenvalue problem. Finally, we solve this well-defined eigenvalue problem to describe the evolution of the perturbations with expressions which are exponential in time. The results tell us how important the parameters (such as the gas permeability, the thermal convection and the diffusion coefficient of oxygen) will be to the onset of thermal convection in waste rock. It should be pointed out that the stability analysis presented in the following section can only characterize the thermal regime up to the critical state, i.e. from conduction state to the onset of convection.

STABILITY ANALYSIS

Governing equations

Coupled heat transfer and gas flow have been studied by many researchers. The governing equations

used in this study were derived by Amter *et al.* [34]. They consist of four equations, a constitutive relation, Darcy's Law, a volume balance, and an energy balance, as follows:

$$\rho = \frac{1}{RT}[P_v\Omega_v + (P - P_v)\Omega_a] \quad (1)$$

$$\mathbf{q} = -\frac{k}{\mu}(\nabla P - g\rho\mathbf{z}) \quad (2)$$

$$\nabla\cdot\mathbf{q} - \mathbf{q}\cdot\left[\left(\frac{1}{T} + \frac{1}{P_a}\frac{dP_v}{dT_a}\right)\nabla T - \frac{1}{P_a}\nabla P\right] = 0 \quad (3)$$

$$K_t\nabla^2 T - c_p^{gas}\rho\mathbf{q}\cdot\nabla T + \left(1 + \frac{P_v}{P_a}\right)\mathbf{q}\cdot\nabla P_a + S_h - \frac{H_v\Omega_v}{RT}\mathbf{q}\cdot\left[\left(1 + \frac{P_v}{P_a}\right)\frac{dP_v}{dT}\nabla T - \frac{P_v}{P_a}\nabla P\right] = c_p^{rock}\rho_{rock}(1-n)\frac{\partial T}{\partial t} \quad (4)$$

where ρ is the gas density, R is the gas constant, T is the temperature, Ω_v and Ω_a are the molar weights of water vapor and dry air, g is the acceleration of gravity, k is the intrinsic permeability of waste rock, μ is the viscosity of the gas, and $\mathbf{z}$ is a downward-pointing unit vector. The constitutive equation (1) implies that fluid is treated as ideal gas.

A volume balance approach is used rather than mass balance because the volume flux of a gas, rather than the mass, is related to the applied forces by Darcy's law. In a vapor saturated and strong non-isothermal system where gas composition varies, mass can not be accurately characterized by the single-phase mass-balance approach. The theoretical base and the rigorous derivation of equation (3) are referred to Ross *et al.* [35] and Bear [36, equation A-24]. In the heat equation (4), K_t is the thermal conductivity of the porous medium, c_p^{gas} is the specific heat of gas at constant pressure, c_p^{rock} is the specific heat of rock, H_v is the heat of vaporization of water, n is the porosity, and S_h is an internal heat source. In this study, we assume that the relative humidity within the waste dump remains at 100% [37, p. 269]; thus the vapor pressure of water P_v depends only on temperature. By definition, we have $P_a = P - P_v$.

The heat balance equation (4) is specialized for a porous medium filled with moist gas [29, 34]. The first term of the left side represents heat conduction, the second represents sensible heat transfer, and the third represents work done when the gas changes volume (to the extent not included in the second term), and the fifth represents latent heat transfer. The right side represents heating of the rock; a term representing heating of the gas in place has been dropped because the density of gas is usually much smaller than that of rock.

For a given heat source distribution and initial and boundary conditions, equations (1)–(4) can be solved for fields of density ρ, pressure P, temperature T and gas flux $\mathbf{q}$.

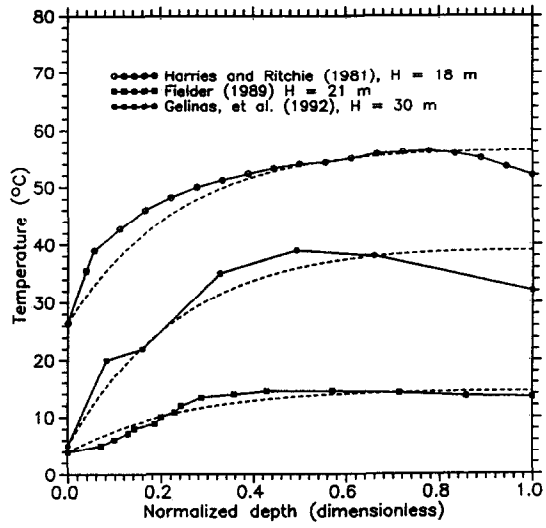

Fig. 2. Measured temperature in waste rock as a function of the waste dump depth (the depth is normalized with respect to the corresponding maximum depth H). Dashed lines are fitted by the analytical solution of equation (7).

Internal heat source

In order to solve the coupled heat transfer and gas flow in waste rock, the heat source term S_h appearing in equation (4) must be identified. The mathematical form of heat production in waste rock is adapted from work by Lefebvre *et al.* [17]. In their study, field measured temperature profiles were used to determine the heat production rate S_h. To do that, a polynomial temperature correlation with depth was first obtained. Using the computed temperature profiles, an analytical solution for one-dimensional heat conduction and convection in the vertical direction was used to determine the heat production rate as a function of depth within the waste. In this analytical model, it is assumed that pyrite oxidation has first-order kinetics with respect to oxygen concentration and that oxygen supply is by diffusion. These assumptions lead to an exponential decline in heat production from the surface. Since the heat production rate is derived from the mean temperature profiles obtained in the field and is directly related to the pyrite oxidation rate and oxygen consumption, the thermal data thus provide the heat production rate independently of chemical or biochemical models.

Studies by Harries and Ritchie [2] and Fielder [1] (Fig. 2) confirmed that the exponential form of heat source is a good approximation. From the mathematical theory of linear ordinary differential equations, equations with an exponential form of source term should lead to a solution with an exponential form as well. Hence, the heat production rate has the following form, Lefebvre *et al.* [17]

$$S_h = S_0\, e^{-\lambda z/H} \quad (5)$$

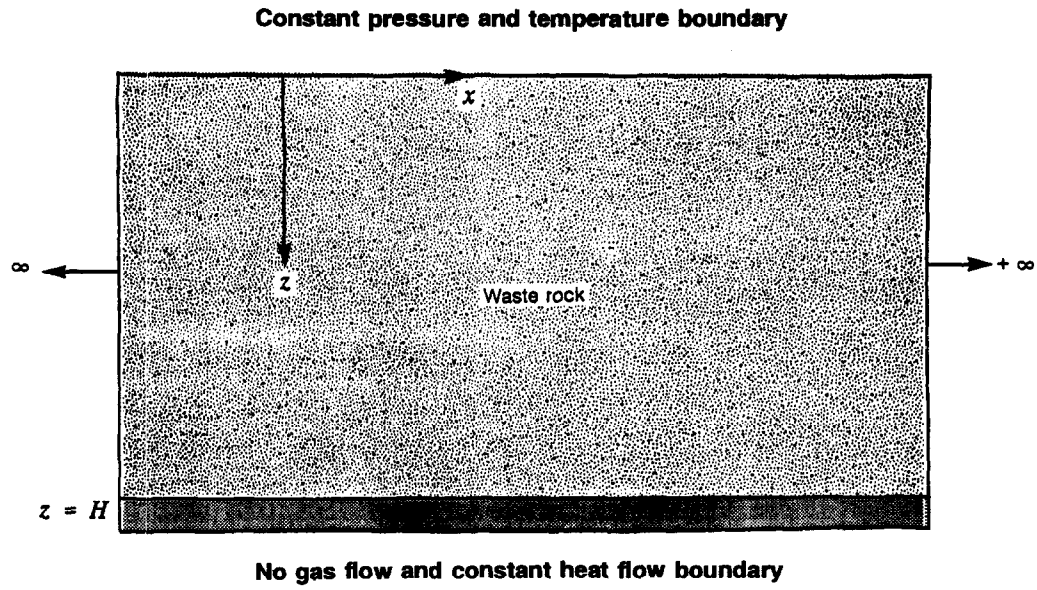

Fig. 3. Geometry and boundary conditions for an infinite horizontal waste dump.

where H is the thickness of the waste dump and λ and S_0 are the heat source constants.

Conduction solution

We start with the static solution of the governing equations (1)–(4). We consider a classical problem of a porous medium bounded by one horizontal, constant heat flux, impermeable plane at the bottom and one isothermal, permeable or impermeable plane at the top as depicted in Fig. 3. This problem is analogous to the Rayleigh–Bénard problem for a viscous fluid and was solved by Horton and Rogers [19] and Lapwood [38] for a porous medium containing a slightly compressible fluid (such a liquid water).

The basic equations governing the physical process are (1), (2), (3), and (4). The boundary conditions are illustrated in Fig. 3 and are defined as

$$T = T_s, \quad P = P_s, \quad \rho = \rho_s, \quad \mathbf{q} = 0 \quad (z = 0)$$

$$\frac{dT}{dz} = \text{const.} = \Gamma_b, \quad \mathbf{q} = 0 \quad (z = H) \tag{6}$$

where the subscript s refers to values at the upper boundary $z = 0$ ($\mathbf{z}$ points downward).

The static solution (denoted by the subscript zero in the unknown variables) is referred to as the "conduction state" and is a function of z only, in which the heat transfer is solely by thermal conduction. Solving equations (4), (5) and (6) using the no-gas-flux condition gives the analytical expression of temperature distribution as

$$T_0 = T_s + \Gamma_b z + \frac{H^2 S_0}{\lambda^2 K_t}\left[1 - e^{-\lambda z/H} - \frac{\lambda z}{H} e^{-\lambda}\right]. \tag{7}$$

Now the system can be described by the hydrostatic equations

$$\mathbf{q}_0 = 0,$$

$$\rho_0 = \frac{\Omega_a}{RT_0}\left[P_0 - P_{v0}\left(1 - \frac{\Omega_v}{\Omega_a}\right)\right]$$

$$\frac{dP_0}{dz} = \rho_0 g = \frac{g\Omega_a}{RT_0}\left[P_0 - P_{v0}\left(1 - \frac{\Omega_v}{\Omega_a}\right)\right],$$

$$P_{v0} = P_{v0}(T_0). \tag{8}$$

Solving the above equations yields the solution for the distribution of P_0:

$$P_0 = P_s e^{g\Omega_a/R\int_0^z 1/T_0 dz} \times\left[1 - \frac{g\Omega_a}{R}\left(1 - \frac{\Omega_v}{\Omega_a}\right)\int_0^z \frac{P_{v0}}{T_0} e^{-g\Omega_a/R\int_0^z 1/T_0 dz}\, dz\right]. \tag{9}$$

Figure 2 also depicts the analytical solutions of temperature described by equation (7) for some specific values of heat source intensity constants and decay constants. By comparing the fitted analytical solution with measured profiles, it can be drawn that the distributed heat source represented by equation (5) yields a reasonably good pattern of temperature distribution.

Perturbation equations and eigenvalue problem

The second step in the stability analysis is to transfer the governing equations into the perturbation equations. We expect from the field observations and the solution of other convective stability problems that the static solution will be unstable if there is a sufficiently large temperature difference within the layer. Let us consider infinitesimal two-dimensional disturbances to the static solution because instability occurs first in two dimensions. The perturbation may be written as

$$\mathbf{q} = \mathbf{q}_0 + \mathbf{q}', \quad P = P_0 + P',$$
$$\rho = \rho_0 + \rho', \quad T = T_0 + T'. \tag{10}$$

Inserting these forms into the system equations (1)–(4), neglecting all second-order perturbation terms and subtracting the static solutions yields

$$\nabla P' + \frac{\mu}{k}\mathbf{q}' - \rho' g \mathbf{z} = 0 \tag{11}$$

$$\nabla \cdot \mathbf{q}' - \mathbf{q}' \cdot \left[\left(\frac{1}{T_0} + \frac{1}{P_{a0}}\frac{dP_{v0}}{dT}\right)\nabla T_0 - \frac{1}{P_{a0}}\nabla P_0\right] = 0, \tag{12}$$

$$K_t \nabla^2 T' - \mathbf{q}' \cdot \left\{c_p^{gas}\rho_0 \nabla T - \frac{1}{c}\left(1 + \frac{P_{v0}}{P_{a0}}\right)\nabla P_{a0} + \frac{H_v \Omega_a}{RT_0}\left[\left(1 + \frac{P_{v0}}{P_{a0}}\right)\frac{dP_v}{dT}\bigg|_{T_0}\nabla T_0 - \frac{P_{v0}}{P_{a0}}\nabla P_0\right]\right\} = c_p^{rock}\rho_{rock}(1-n)\frac{\partial T'}{\partial t} \tag{13}$$

$$\rho' = \frac{\Omega_a}{RT_0}\left[P' - P_v'\left(1 - \frac{\Omega_v}{\Omega_a}\right)\right] - \frac{\Omega_a T'}{RT_0^2}\left[P_0 - P_{v0}\left(1 - \frac{\Omega_v}{\Omega_a}\right)\right] = \frac{\Omega_a}{RT_0}P' - \frac{\Omega_a T'}{RT_0^2}\left[P_0 + \left(T_0\frac{dP_v}{dT}\bigg|_{T_0} - P_{v0}\right)\left(1 - \frac{\Omega_v}{\Omega_a}\right)\right]. \tag{14}$$

Because all coefficients here are independent of x and t, and the boundary conditions encountered in this study are assumed to be independent of x and t, according to the theory of linear ordinary differential equations with constant coefficients, the solution can be expressed in the form of an exponential in the variables x and t. Hence we have

$$(P', \rho', T') = Re[(\hat{P}(z), \hat{\rho}(z), \hat{T}(z))\, e^{ilx + \gamma t}]$$
$$\mathbf{q}' = Re[(u(z), w(z))\, e^{ilx + \gamma t}] \tag{15}$$

where l is the horizontal wave number and γ is the rate of increase in the size of the fluctuation component with wave number l. With the above form of the solution, the system can be reduced to two equations for the unknown vertical flux and temperature:

$$\left(\frac{d^2}{dz^2} - \frac{A_0 + E_0}{H}\frac{d}{dz} - \frac{1}{H}\frac{dA_0}{dz} + \frac{A_0 E_0}{H^2} - l^2\right) \times w = \frac{gP_s\Omega_a l^2 k}{\mu R T_s^2} F_0 \hat{T} \tag{16}$$

$$\left(K_t\frac{d^2}{dz^2} - D_0 - l^2 K_t\right)\hat{T} = \frac{\rho_s c_p^{gas}\Delta T}{H} B_0 w \tag{17}$$

with dimensionless z-dependent quantities denoted as

$$A_0 = H\left(\frac{1}{T_0} + \frac{1}{P_{a0}}\frac{dP_v}{dT}\bigg|_{T_0}\right)\frac{dP_v}{dT}\bigg|_{T_0} - \frac{H}{P_{a0}}\frac{dP}{dz} \tag{18}$$

$$B_0 = \frac{\rho_0}{\rho_s}\frac{H}{T_s}\frac{dT_0}{dz} - \frac{\lambda_1 H}{P_s}\left(1 + \frac{P_{v0}}{P_{a0}}\right)\frac{dP_{a0}}{dz} + \frac{\lambda_2 H}{P_s}\frac{T_s}{T_0}\left[\left(1 + \frac{P_{v0}}{P_{a0}}\right)\frac{dP_{v0}}{dT}\bigg|_{T_0}\frac{dT_0}{dz} - \frac{P_{v0}}{P_{a0}}\frac{dP_{a0}}{dz}\right]$$
$$\lambda_1 = \frac{P_s}{c c_p^{gas}\rho_s T_s},$$
$$\lambda_2 = \frac{H_v \Omega_v P_s}{c_p^{gas}\rho_s R (T_s)^2} \tag{19}$$

$$E_0 = \frac{gH\Omega_a}{RT_0} \tag{20}$$

$$F_0 = \frac{T_s^2}{P_s T_0}\left[\left(\frac{dP_v}{dT}\bigg|_{T_0} - \frac{P_v}{T_0}\right)\left(1 - \frac{\Omega_v}{\Omega_a}\right) + \frac{P_v}{T_0}\right] \tag{21}$$

and the parameter that is related to the time constant

$$D_0 = \gamma c_p^{rock}\rho_{rock}(1-n). \tag{22}$$

Each of the quantities defined in equations (18)–(21) can be interpreted physically. The quantity A_0 reflects the effect of gas compressibility as shown in Fig. 4. It is zero for a dry gas when the thermal gradient equals to the self-convective gradient or $g\Omega/R$. The quantity A_0 increases to a value on the order of one (more compressible) as the z value tends to the top boundary where the maximum temperature gradient may occur. The quantity B_0 represents the buoyancy force driven by sensible heat convection, latent heat convection, and change of gas volume. It is zero when there is no temperature gradient (at the bottom), and reaches its maximum somewhere in the upper portion of the dump. The quantity E_0 represents the gas density change due to the pressure fluctuation. In the absence of forced convection and at the Earth's surface E_0 is negligibly small. Finally, the quantity F_0 reflects the enhancement of temperature-caused density change due to the presence of vapor. For the temperatures considered in this study, it starts from near 1 (at the upper boundary) and increases monotonically as the temperature increases (tends to the bottom surface).

It is convenient to nondimensionalize equations (16) and (17) by introducing

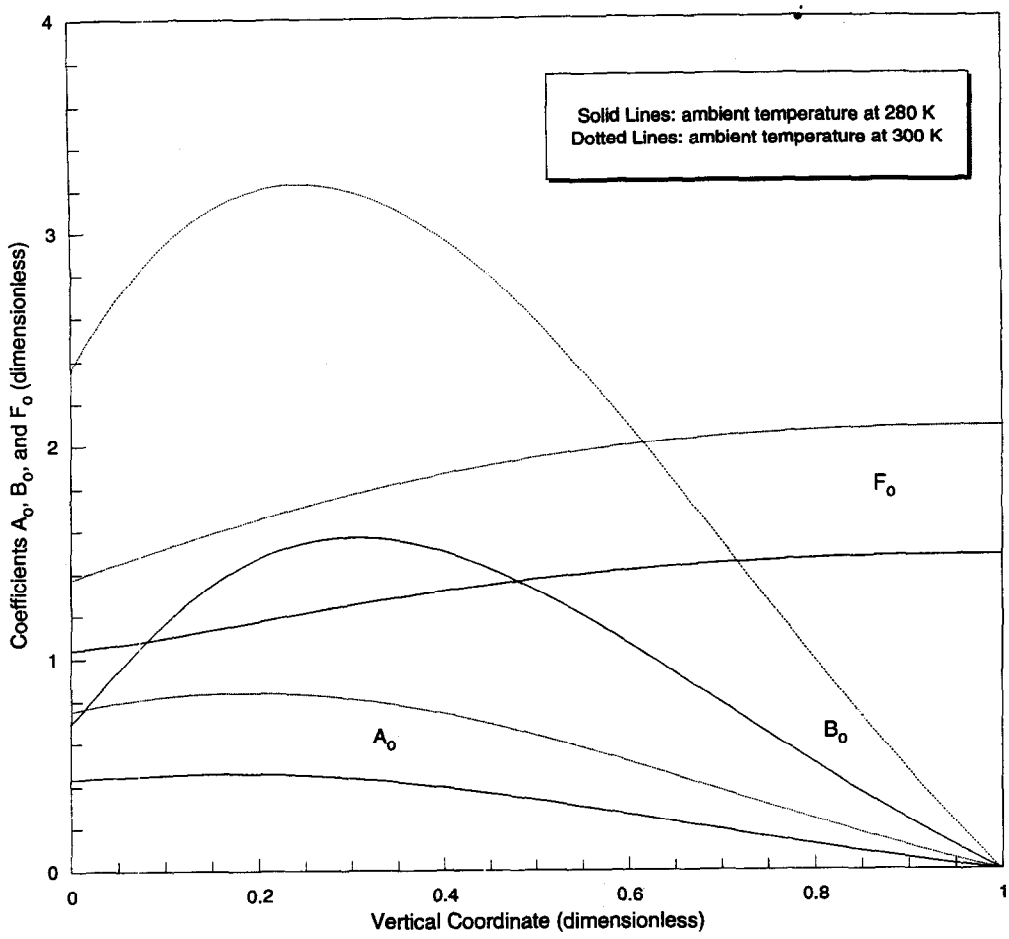

Fig. 4. Illustration of the dimensionless quantities A_0, B_0 and F_0 as functions of depth of a waste dump. The maximum temperature difference under both ambient temperatures reaches 40 K in the dump.

$$\bar{l}=\frac{l}{H},\quad \zeta=\frac{z}{H},\quad \bar{w}=\frac{\rho_s H c_p^{gas}}{K_t}w,$$

$$\theta=\frac{\hat{T}}{T_b-T_s},\quad \bar{D}=\frac{H^2 D_0}{K_t}. \tag{23}$$

Equations (17) and (18) then become

$$\left(\frac{d^2}{d\zeta^2}-\bar{D}-\bar{l}^2\right)\theta=B_0\bar{w}, \tag{24}$$

$$\left(\frac{d^2}{d\zeta^2}-(A_0+E_0)\frac{d}{d\zeta}-\frac{dA_0}{d\zeta}+A_0E_0-\bar{l}^2\right)\bar{w}=R_a\bar{l}^2F_0\theta \tag{25}$$

with the system Rayleigh number redefined for waste rock as

$$R_a=\frac{gH\rho_s P_s\Omega_a c_p^{gas}k}{\mu K_t RT_s}. \tag{26}$$

Equations (24) and (25) together with certain boundary conditions in their dimensionless form can define an eigenvalue problem for the system's Rayleigh number R_a.

Onset condition

As described earlier, the third step in the stability analysis involves defining and solving the eigenvalue problem. The corresponding boundary condition is

$$\theta=0,\quad \frac{d\bar{w}}{d\zeta}=0;\quad (\zeta=0)$$

$$\frac{d\theta}{d\zeta}=0,\quad \bar{w}=0;\quad (\zeta=1). \tag{27}$$

Now the eigenvalue problem is well defined by equations (24), (25) and (27).

The coefficients A_0, B_0, E_0 and F_0 which appear in equations (24) and (25) are functions of ζ which can be evaluated by equations (18)–(21). The dependence of A_0, B_0 and F_0 on temperature is illustrated in Fig. 4. The coefficients A_0 and F_0 vary linearly with the

vertical coordinate ζ, but B_0, representing the vapor pressure effect, is highly nonlinear and changes quickly as the vertical coordinate increases. The solution of equations (24), (25) and (27) leads to an eigenvalue problem (Appendix A) defined by a system of k homogeneous equations as

$$\sum_{k=0}^{\infty} \Pi_{jk}\Theta_k = 0$$

$$\Pi_{jk} = (\bar{D}+j^2\pi^2+\bar{l}^2)\delta_{jk} + 2R_a\bar{l}^2\int_0^1 B_0 W_k \sin\left(j-\frac{1}{2}\right)\pi\zeta \, d\zeta, \quad (28)$$

where Θ_k is the coefficient of temperature solution, δ_{jk} is the Kronecker tensor and W_k is the solution function of vertical flux.

A nontrivial solution exists when the determinant of the matrix of coefficients Π_{jk} vanishes, i.e.

$$\|\Pi_{jk}\| = 0. \quad (29)$$

This is a kth rank eigenvalue problem. A first rank solution of the eigenvalue problem will be given by setting k equal to 1 and Π_{11} equal to zero and ignoring all the others. This corresponds to the choice of $\sin(\pi\zeta/2)$ as a trial function for θ. Similarly, by introducing additional terms in the expansion for θ, we will expect to get a more accurate solution for R_a. For the kth rank solution, equation (29) forms a kth rank determinant and can only be solved numerically for $k > 3$ in order to obtain the system's eigenvalues and the corresponding eigenfunctions. Because it is expected that the higher rank modes will not play as important a role as the lower rank modes [18, 26], calculations with second-order approximations should give a good approximation of the stability of the system. The corresponding result for the second rank is

$$\begin{vmatrix} \Pi_{11} & \Pi_{12} \\ \Pi_{21} & \Pi_{22} \end{vmatrix} =$$

$$\begin{vmatrix} \bar{D}+\frac{\pi^2}{4}+\bar{l}^2+2R_a\bar{l}^2 I_{11} & 2R_a\bar{l}^2 I_{12} \\ 2R_a\bar{l}^2 I_{21} & \bar{D}+\frac{9}{4}\pi^2+\bar{l}^2+2R_a\bar{l}^2 I_{22} \end{vmatrix} = 0$$

$$I_{ij} = \int_0^1 B_0 W_i \sin\left(j-\frac{1}{2}\right)\pi\zeta \, d\zeta. \quad (30)$$

The above condition gives the critical Rayleigh numbers corresponding to the first and the second instability modes

Analysis

When a system's Rayleigh number is equal to the critical Rayleigh number the system is at the threshold of convection. Figure 5 shows the temperature field and streamfunction corresponding to the second rank eigenvalue problem with heat source constants $S_0 = 0.072\ \mathrm{J\,m^{-3}\,s^{-1}}$ and $\lambda = 1.78$. Figures 5(a, b) are streamfunction and temperature fields for the first mode, while Figure 5(c, d) are for the second mode. These streamfunctions and temperature isotherms are eigenfunctions and represent the patterns of air flow and temperature distribution when a system's Rayleigh number reaches the first and second critical Rayleigh numbers as shown in equation (31).

Under the ideal condition, each system has only one Rayleigh number. A system's Rayleigh number for a waste rock system is defined by equation (26). Its value is linearly proportional to the system's parameters, namely, the gravity constant g, the thickness of the waste dump H, the gas density ρ_s, the gas pressure P_s at the top surface, the molar weight of gas Ω_a, the specific heat of gas c_p^{gas} and the intrinsic gas permeability k, but the value of the system's Rayleigh number is inversely proportional to the other system parameters: the viscosity of gas μ, the thermal conductivity of the rock K_t, the gas constant R and the top surface temperature T_s. Therefore, it is a constant for a given waste rock dump. The critical Rayleigh numbers, on the other hand, depend on the dimensionless quantities, A_0, B_0, E_0 and F_0 which are not only functions of the system's parameters, but also are strong functions of heat source constants. In general, because the strength of the heat source changes during the process of acid generation, the critical Rayleigh numbers changes as time passes. If some critical Rayleigh numbers decrease to equal or less than the system's Rayleigh number, the instability will occur and the convective gas flow with patterns characterized by Fig. 5 will be onset in the waste dump.

Figure 6 illustrates the critical Rayleigh number as a function of the horizontal wave number for different values of the maximum temperature occurring in waste rock by using equations (29) and (31). The critical Rayleigh number is that at which the critical curve reaches its minimum. For a waste dump reaching a specified maximum temperature, if the Rayleigh number is in the region above the corresponding critical curve, the system will be unstable and will form convection cells. Because of the nonlinear dependence of vapor pressure on temperature, the higher the maximum temperature is (for a fixed temperature difference between the maximum and the ambient), the lower the critical Rayleigh number will be and

$$R_{a1,2}^{*} = -\frac{[(\pi^2+4l^2)I_{22}+(9\pi^2+4l^2)I_{11}]-+\sqrt{[(9\pi^2+4l^2)I_{11}-(\pi^2+4l^2)I_{22}]^2+4(\pi^2+4l^2)(9\pi^2+4l^2)I_{12}I_{21}}}{16\bar{l}^2(I_{11}I_{22}-I_{12}I_{21})}. \quad (31)$$

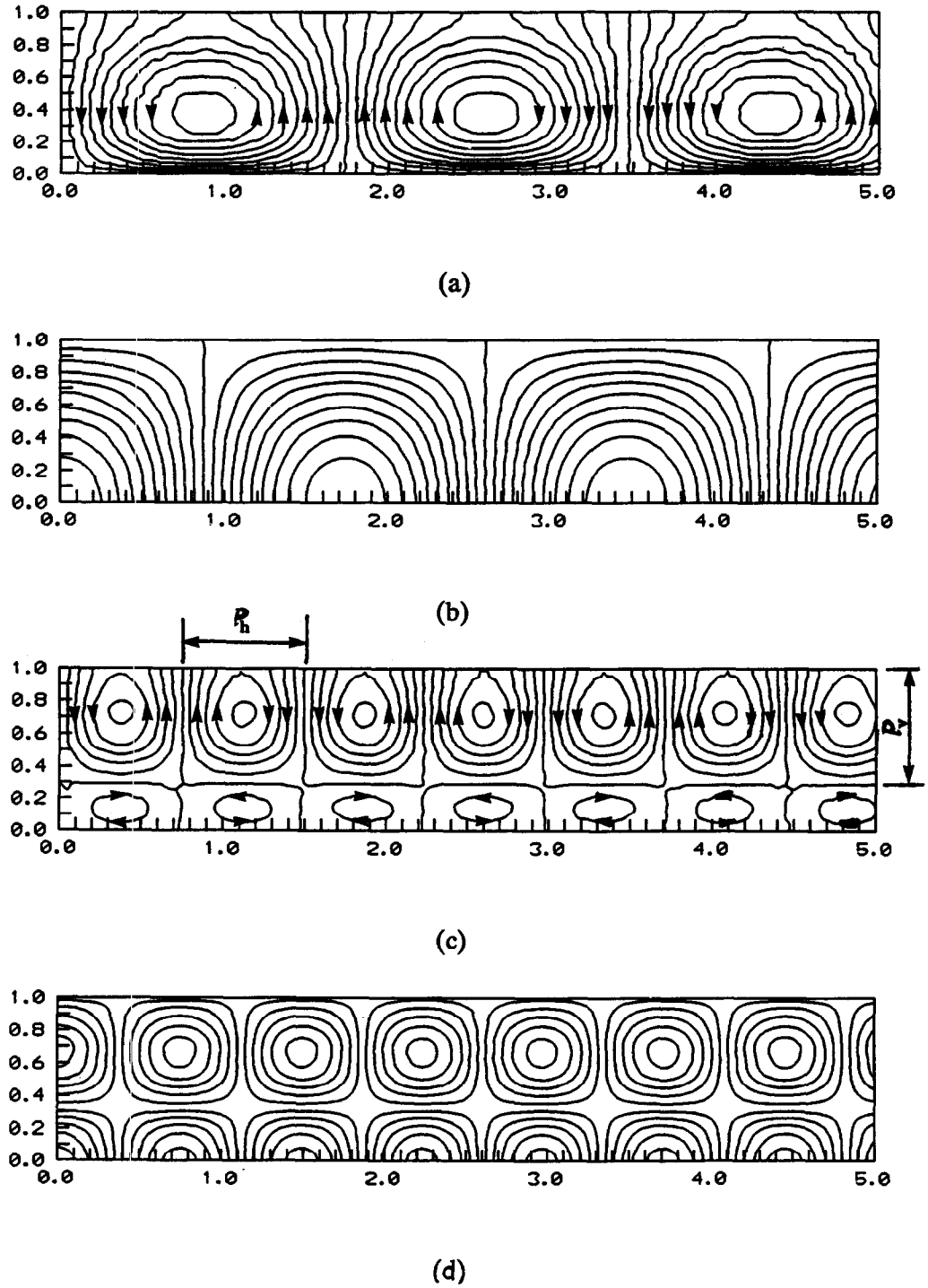

Fig. 5. Streamfunctions and temperature isotherms for a second rank eigenvalue problem with the top surface open to the atmosphere: (a) streamfunctions for the first instability mode; (b) temperature isotherms for the first instability mode; (c) streamfunctions for the second instability mode; (d) temperature isotherms for the second instability mode. The heat source intensity constant $S_0 = 0.072$ J m^{-3} s^{-1}, the heat source decay rate $\lambda = 1.7$ and the ambient temperature 280 K are used. Such a heat source will create a 60 K temperature difference in the dump.

the higher the ambient temperature is, the lower the critical Rayleigh number will be.

To illustrate the convection onset process, consider the following hypothetical scenario. At the initial state, when waste rock is newly dumped, gas pressures within the rocks are in the static condition and no oxidation has taken place. Temperature distribution within the waste rock is relatively uniform and tem-

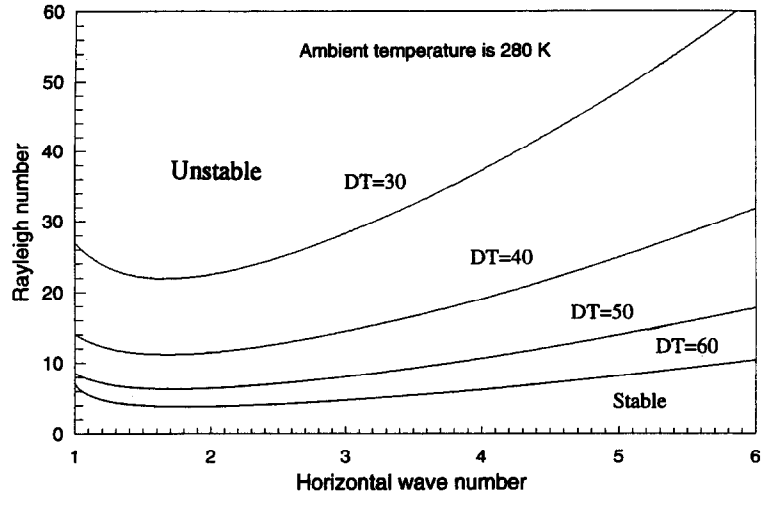

(a)

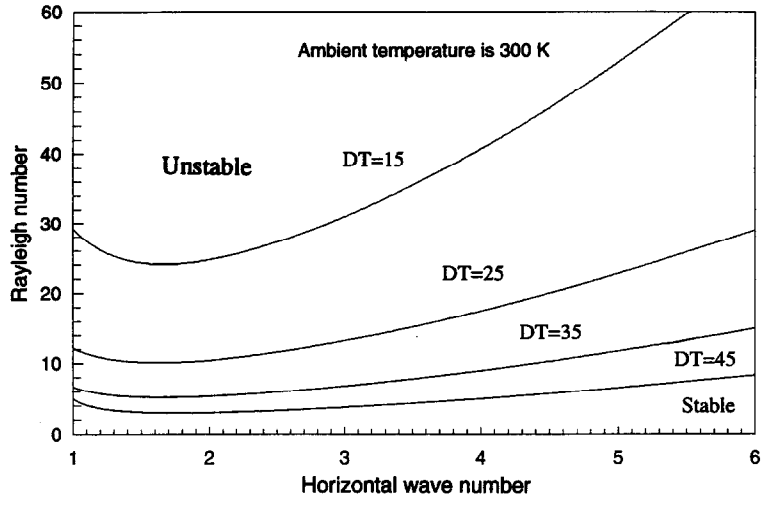

(b)

Fig. 6. The critical Rayleigh number as a function of the horizontal wave number and the maximum temperature difference with: (a) the ambient temperature at 280 K; (b) the ambient temperature at 300 K.

perature gradients are almost zero. Therefore, the critical Rayleigh numbers are expected to be much larger than the system's Rayleigh number R_a. As oxygen diffuses into the rocks, pyritic materials start to oxidize and temperature gradients begin to build up. At the early stage, conduction will dominate within the rocks and distributions of temperature and pressure can be described by equations (8) and (9). As temperatures in the dump increase, the first critical Rayleigh number decreases. When the temperature gradients are sufficiently large so that the first critical Rayleigh number is lowered to less than or equal to the system's Rayleigh number, the convection begins. The patterns of convection cells and temperature distribution at this threshold moment can be characterized by corresponding eigenfunctions and are shown in Fig. 5(a, b). At this stage, only one layer of convection cells exists in the waste dump. Because the top is open to the atmosphere, convective gas circulation will bring more oxygen into the waste dump and enhance the pyrite oxidation.

As the pyrite oxidation accelerates, temperature gradients may increase to a further sufficient high level and the second critical Rayleigh number may drop to the value of the system Rayleigh number. At this point, the second mode may be amplified and convective gas flow may shift to the pattern as illustrated in Fig. 5(c, d). Two layers of convection cells within the dump will be observed, the upper layer cells are connected to the atmosphere and the bottom layer cells are self-closed. Since we have an open system at the top surface, the upper layer will directly promote the circulation of oxygen and gas will flow in and out freely through the surface. If temperature gradients

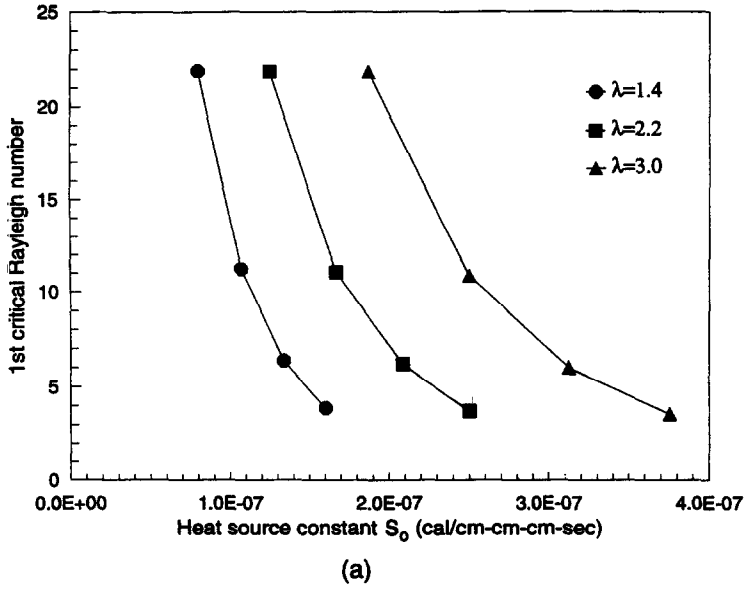

(a)

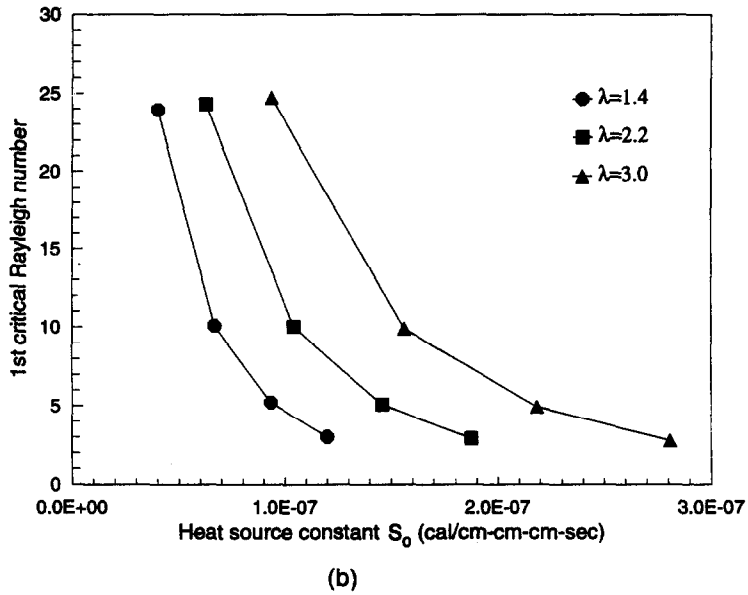

(b)

Fig. 7. The critical Rayleigh number for the first mode as a function of the heat source constants S_0 and λ with: (a) the ambient temperature at 280 K; (b) the ambient temperature at 300 K. The distributed heat source is defined as $S_h = S_0 e^{-\lambda \zeta}$.

continue to increase, at some point (ample physical and numerical experiments indicate that this is generally at the third instability mode), heat transfer will enter a chaotic regime.

To examine the effect of the surface ambient temperature, we analyze the stability conditions at two different ambient atmospheric temperatures, one at 280 K and the other at 300 K. These differences are illustrated in Figs. 7–8. In general, the lower the ambient temperature is, the lower the critical Rayleigh number (if the waste rock reaches the same maximum temperature). For example, for maximum temperature of 325 K (Fig. 6 and Table 2) the Rayleigh number reaches its minimum value of 8.28 for the ambient temperature of 280 K and reaches its maximum value of 10.1 for the ambient temperature of 300 K. Therefore, a waste rock under a lower ambient temperature tends to be less stable. On the other hand, if the temperature difference between the maximum and the ambient remains constant, a waste rock with a higher ambient temperature condition tends to be less stable. For example, if the temperature difference is 40 K, the critical Rayleigh number for a waste rock with an ambient temperature of 280 K will be 11.10, while the critical Rayleigh number for an ambient temperature of 300 K will be only 3.87. This

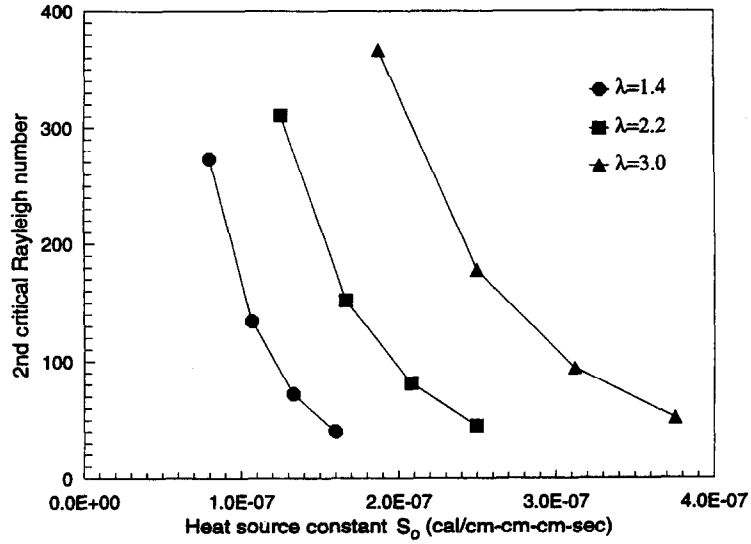

(a)

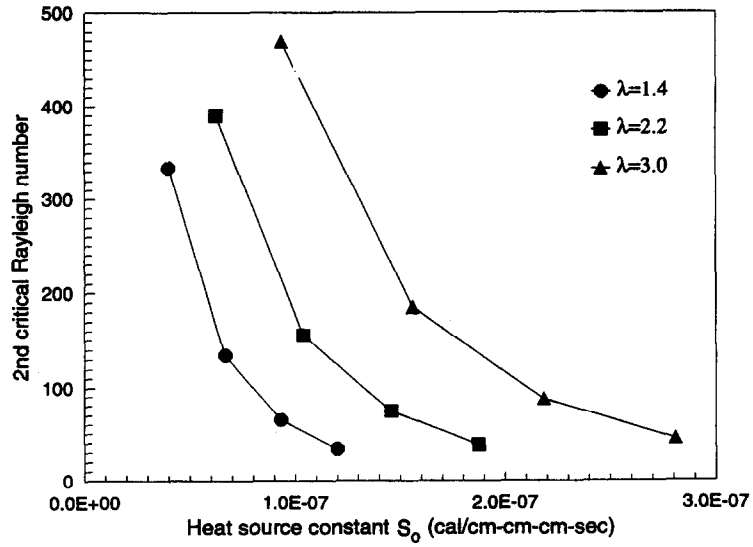

(b)

Fig. 8. The critical Rayleigh number for the second mode as a function of the heat source constants S_0 and λ with: (a) the ambient temperature at 280 K; (b) the ambient temperature at 300 K. The distributed heat source is defined as $S_h = S_0 e^{-\lambda\zeta}$.

Table 1. Parameters used in the stability analysis

c_p^{gas}	58 J kg^{-1} K^{-1}	K_t	1.2 J K^{-1} m^{-1} s^{-1}	μ	1.86×10^{-5} kg m^{-1} s^{-1}
c_p^{rock}	60 J kg^{-1} K^{-1}	n	3.0×10^{-1} dimensionless	ρ_s	1.0 kg m^{-3}
g	9.8 m s^{-2}	P_s	8.88×10^{4} kg m^{-1} s^{-1}	ρ_{rock}	3000 kg m^{-3}
H	<30 m	R	8.314 kg m^2 s^{-2} mol^{-1} K^{-1}	Ω_a	2.9×10^{-4} kg mol^{-1}
H_v	2.45×10^{6} J kg^{-1}	T_s	280, 300 K	Ω_v	1.8×10^{-4} kg mol^{-1}
k	10^{-9} m^2	ΔT	15–55 K		
S_0	0.024–0.096 J m^{-3} s^{-1}	λ	1.0–3.0 dimensionless		

means, for instance, a waste rock with Rayleigh number $R_a = 5.0$ will be unstable if it is under a 300 K ambient temperature, and there will be no convective flow (stable) if it is under 280 K ambient temperature.

Table 2. The critical Rayleigh numbers and σ (the ratio of the vertical cell length l_v to the horizonal cell length l_h as depicted in Fig. 5) as functions of the maximum temperature, boundary constraints, and the ambient temperatures. The heat source decay constant is specified as $\lambda = 1.7$ in all calculations

Temperature difference ΔT (K)	Ambient temperature 280 K				Ambient temperature at 300 K			
	1st mode		2nd mode		1st mode		2nd mode	
	R_a^*	σ	$R_a^\dagger$	σ	R_a^*	σ	$R_a^\dagger$	σ
25	32.4	1.68	429.6	4.21	10.1	1.63	141.6	4.15
30	21.9	1.67	285.3	4.24	7.09	1.63	97.0	4.19
35	15.4	1.67	197.1	4.28	5.17	1.66	68.3	4.22
40	11.1	1.68	140.2	4.31	3.87	1.71	48.9	4.27
45	8.28	1.69	101.9	4.34	2.96	1.78	35.2	4.31

To estimate the time constant for the growth of a fluctuation, we can examine the case where the Rayleigh number of a system is twice the critical Rayleigh number and the horizontal wave number is that of the first mode. Hence, we can obtain a dimensionless increases rate $\bar{D}$ by solving equation (30). The rate of the growth of the fluctuation can be estimated as

$$\gamma = \frac{K_t \bar{D}}{c_p^{\text{rock}} \rho_{\text{rock}} (1-n) H^2}. \tag{32}$$

We further assume that the thickness of the layer is 30 m, the air permeability is 10^{-9} m^2 and the other system parameters are listed in Table 1. Solving $\bar{D}$ with equation (30) and substituting it into equation (32) yields γ as 1/2.9 years^{-1}. This indicates that in a system with a Rayleigh number twice the critical value, fluctuations will grow by a factor of e every 2.9 years. The convection cell pattern is illustrated in Fig. 5(a) with the cell length about 50 m.

Comparison with other studies

We will shown in this section that the above results are qualitatively consistent with some field observations. Strong convective gas flow has been found and monitored at the South Dump of La Mine Doyon, Quebec [3, 17]. The dump has similar parameters to the above case. It has an area of about 1000 m × 600 m with 30–35 m in depth. Using the parameters described above and listed in Table 1, the system Rayleigh number R_a can be determined by equation (26) as 8.381 for the atmospheric temperature at 280 K. The critical Rayleigh numbers, on the other hand, are calculated by equation (31) as $R_a^* = 3.76$ for the first mode and $R_a^\dagger = 42.93$ for the second mode. Therefore, according to the theory, convective gas flow will occur and the system will be in its first mode as depicted by Fig. 5(a). This dump is about 10 years old and was observed to start to produce acid about 3 years after waste rock was in place and reached the peak value of acid generation at about 5 years. From that time, strong convective gas flow has been observed. This time scale is comparable with the calculated value of 2.9 years. Field measurement of surface temperature distribution along the dump width direction showed that the surface temperature varies periodically with a wave length of about 15 m, which is on the same order of magnitude with the values predicted by the theory. The theoretical results predict the wave length is about 50 m for the first mode and about 20 m for the second mode. Counter-flow also was observed in some boreholes. This implies that the second instability mode could occur within the dump. This is possible if the air permeability is slightly more than five times as large as the used value of 10^{-9} m^2. In such case, the system's Rayleigh number is greater than the second critical Rayleigh number of 42.93 and the system will be on the second mode as depicted in Fig. 5(c). If only the gas permeability changes to 10^{-10} m^2 and the other parameters remain unchanged, the system's Rayleigh number determined by equation (26) is $R_a = 0.8381$. According to the theory, there should be no convection in waste rock and the system is in stable condition because $R_a = 0.8381 < R_a^* = 3.76$. The threshold permeability value of 10^{-10} m^2 is qualitatively in agreement with the conclusion from the study by Bennett *et al.* [4].

DISCUSSIONS AND CONCLUSIONS

Equations (30)–(31) have some limitations in that they can only be directly used for large temperature difference, say, greater than 10 K. Although the presented theoretical framework itself is not limited to a smaller temperature difference, the limitation will be introduced when one tries to use the second rank eigenvalue expansion to evaluate the general theoretical result (equation (29)). Our numerical experiments tell that for temperature difference less than 10 K, a higher rank expansion is more plausible in order to ensure accurate predictions.

Another uncertainty on directly applying the theoretical results is on the choice of source strength constants S_0 and λ. Based on the assumption of pure oxygen diffusion, Gelinas *et al.* [3] and Lefebvre *et al.* [17] provide mathematical expressions of the source strength constants in terms of some chemical parameters such as the oxidation rate, diffusion coefficient, etc. On the other hand, a simple analysis using these expressions and the conduction solution (7) reveals that oxygen diffusion itself can cause temperature increase to about 15 K under the most favorable condition. Other mechanisms such as pref-

erential flow paths through large porous space, periodic barometric pumping, bacteria related chemical reactions, and fermentation reactions could also contribute to the heat generation deep in waste rock. Therefore, future study on identifying heat source mechanism and quantifying the strength in terms of physical and chemical parameters is crucial in applying the present theoretical work and in predicting acid generation.

A mine waste dump in which active oxidation of pyritic materials occurs can generate a large amount of heat, creating large thermal gradients within waste rock. Gas in the highly porous, unsaturated waste rock may form convection cells.

Our stability analysis provides an analytical means to examine thermal regime in waste rock and determine under what conditions a waste dump will be dominated by conduction or convection. Potential patterns of flow of the thermal convection cells at the threshold of onset are also given by stability analysis; it is illustrated in Fig. 5.

The system's Rayleigh number is the key indicator in analysis of stability problems. This parameter must be redefined for the waste rock problem (equation (26)). If the critical Rayleigh number is smaller than the system Rayleigh number, convection will not occur and thermal conduction will be the dominating mechanism for heat transfer. On the other hand, if the critical Rayleigh number reaches or exceeds the system Rayleigh number, convective flow will be significant. The critical Rayleigh number for a system, filled with a moist gas is more complicated than in the previously solved cases of a liquid-saturated system, and a dry gas. The presence of a distributed heat source in waste rock further complicates the thermal convection process. The critical Rayleigh number depends on four dimensionless quantities A_0, B_0, E_0 and F_0 defined in equations (18)–(21). These dimensionless quantities reflect the nature of the upper boundary, the atmospheric temperature, the strength of the heat source and the vapor pressure. The onset of thermal convection in a two-dimensional, infinite horizontal layer of waste rock filled with moist gas has been found by perturbation analysis. Our analysis demonstrates that convective gas flow will occur for a typical-size mine waste dump under the conditions examined in this study. Results from the stability analysis show that the maximum temperature in a waste rock depends on the ambient atmospheric temperature, the strength of the heat source, and the nature of the upper boundary. Lower ambient temperature will make convection much more likely to occur. The conditions for occurrence of convective flow, the convection cell shape, and the timing for the open case are consistent with some field measurements and numerical studies.

REFERENCES

1. Fielder, D., Identification of acid producing zones within a reclaimed surface mine utilizing thermal surveying. M.S. thesis, Geosciences Department, Pennsylvania State University, PA, 1989, p. 32.
2. Harries, J. R. and Ritchie, A. I. M., The use of temperature profiles to estimate the pyritic oxidation rate in a waste rock dump from an open cut mine, *Water, Air and Soil Pollution*, 1981, **15**, 405–423.
3. Gélinas, P., Lefebvre, R. and Choquette, M., Monitoring of acid mine drainage in a waste rock dump. Geological Engineering Department, University of Laval, Quebec, 1992.
4. Bennett, J. W., Harries, J. R., Pantelis, G. and Ritchie, A. I. M., Limitations on pyrite oxidation rates in dumps set by air transport mechanisms. *International Symposium on Biohydrometallurgy*, Jacksons Holes, Wyoming, August 13–18, 1990.
5. Guo, W. and Parizek, R. R., Research on thermal anomalies indicating acid reactions in mine spoil and temperature prediction by numerical model. Geosciences Department, Pennsylvania State University, PA, August, 1992, p. 53.
6. Harries, J. R., Development of a theoretical approach to the heap leaching of copper sulphic ores. *Proceedings of the Australian Institute of Mining and Metallurgy*, 1969, **230**, pp. 81–92.
7. Ross, B., Amter, S. and Lu, N., Numerical studies of rock-gas flow in Yucca Mountain. Sandia National Laboratories Report, SAND91-7034, 1992.
8. Temple, K. L. and Koehler, W. A., Drainage from bituminous coal mines. *West Virginia University Agricultural Experiment Station Research Bulletin*, 1959, No. 25.
9. Lorenz, W. C. and Tarpley, E. C., Oxidation of coal mine pyrite. US Bureau of Mines Report, Inv. 6247, Pittsburgh, PA, 1963.
10. Cathles, L. M. and Apps, J. A., A model of the dump leaching process that incorporates oxygen balance, heat balance, and air convection. *Metallurgical Transactions B*, 1975, **6b**, 617–624.
11. Pantelis, D. and Ritchie, A. I. M., Macroscopic transport mechanisms as a rate-limiting factor in dump leaching of pyrite ores. *Applied Mathematics Modelling*, 1991, **15**, 136–143.
12. Morth, A. H., Smith, E. E. and Shumate, K. A., Pyritic systems: a mathematical model. EPA Technology Series Report no. 665771, Washington D.C., 1972, p. 172.
13. Ritchie, A. I. M., Mathematical models for pyrite oxidation, Report AAEC/E429, 1977.
14. Jaynes, D. B., Rogowski, A. S. and Pionke, H. B., Acid mine drainage from reclaimed coal strip mines, I. Model description. *Water Resources Research*, 1984, **20**, 233–250.
15. Davis, G. B. and Ritchie, A. I. M., A model of oxidation in pyritic mine wastes: part 1 equations and approximate solution. *Applied Mathematics Modelling*, 1986, **10**, 314–322.
16. Nicholson, R. V., A review of models to predict acid generation rates in sulphide waste rock at mine sites. *International Workshop on Waste Rock Modelling*, Toronto, Canada, Sept. 29–Oct. 1, 1992.
17. Lefebvre, R., Gélinas, P. Isabel, D., Heat transfer analysis applied to acid mine drainage production in a waste rock dump, La Mine Doyson (Quebec). *International Association of Hydrogeology*, Hamilton, 1992.
18. Rayleigh, Lord, On convection currents in a horizontal layer of fluid when the higher temperature is on the under side. *Philosophical Magazine*, 1916, **6**(32), 529–546.
19. Horton, C. W. and Rogers, F. T., Convection currents in a porous medium. *Journal of Applied Physics*, **16**, 367–370.
20. Nield, D. A., Onset of convection in a porous layer saturated by an ideal gas. *International Journal of Heat and Mass Transfer*, 1982, **25**, 1605–1606.
21. Kaviany, M., Thermal convective instabilities in a porous medium. *ASME Journal of Heat Transfer*, 1984a, **106**, 137–142.

22. Kaviany, M., Onset of thermal convection in a saturated porous medium: experiment and analysis. *International Journal of Heat and Mass Transfer*, 1984b, **27**, 2101–2110.
23. Plumb, O. A., Drying complex porous materials–modelling and experiments. *Convective Heat and Mass Transfer in Porous Media*, ed. S. Kakaç, B. Kilkiş, F. A. Kulacki and F. Arinç. Kluwer Academic, Dordecht, 1991, pp. 963–984.
24. Bories, S. S., Fundamentals of drying capillary-porous bodies. *Convective Heat and Mass Transfer in Porous Media*, ed. S. Kakaç, B. Kilkiş, F. A. Kulacki and F. Arinç. Kluwer Academic, Dordecht,1991, pp. 77–141.
25. Tien, C. L. and Vafai. K., Convective and radiative heat transfer in porous media. In *Advances in Applied Mechanics*, 1990, **27**, 225–281.
26. Nield, D. A. and Bejan, A., *Convection in Porous Media*, Springer, Berlin, 1992.
27. Saatdjian, E., Natural convection in a porous layer saturated with a compressible ideal gas. *International Journal of Heat and Mass Transfer*, 1980, **23**, 1681–1683.
28. Tsang, Y. W. and Pruess, K., A study of thermal induced convection near a high-level nuclear waste repository in partially saturated fractured tuff. *Water Resources Research*, 1987, **23**, 1958–1966.
29. Zhang, Y., Lu, N. and Ross, B., Convective instability of moist gas in a porous medium. *International Journal of Heat and Mass Transfer*, 1994, **37**, 129–138.
30. Powers, D., O'Neill, K. and Colbeck, C., Theory of nature convection in snow. *Journal of Geophysical Research*, 1985, **90**(D6), 10641–10649.
31. Ross, B., Zhang, Y. and Lu, N., Implications of stability analysis for heat transfer at Yucca Mountain. *International Conference on High Level Radioactive Waste Management*, Las Vegas, April, 1993.
32. Chandrasekhar, S., *Hydrodynamic and Hydromagnetic Stability*. Dover Publications, New York, 1961. p. 652.
33. Phillips, O. M., *Flow and Reactions in Permeable Rocks*. Cambridge University Press, Cambridge, 1991.
34. Amter, S., Lu, N. and Ross, B., Thermally driven gas flow beneath Yucca Mountain, Nevada. In *Multiphase Transport in Porous Media*, ed. R. R. Eaton *et al.* American Society of Mechanical Engineers, New York, 1991, pp. 17–24.
35. Ross, B., Amter, S. and Lu, N., Numerical studies of rock-gas flow in Yucca Mountain, Sandia National Laboratories Report, SAND91-7034, 1992.
36. Bear, J., *Hydraulics of Groundwater*. McGraw-Hill, New York, 1979.
37. Hillel, D., *Fundamentals of Soil Physics*. Academic Press, New York, 1980.
38. Lapwood, E. R., Convection of a fluid in a porous medium, *Proceedings of the Cambridge Philosophical Society*, 1948, **44**, 508.
39. Mathews, J. and Walker, R. L., *Mathematical Methods of Physics*. W. A. Benjamin, New York, 1970, p. 501.

APPENDIX A

Because the boundary conditions (27) require no temperature perturbation on the top and no heat flow on the bottom surfaces, we can assume a general solution for the temperature field in the form of

$$\theta = \Sigma_j \Theta_j \sin(j-\tfrac{1}{2})\pi\zeta. \tag{A1}$$

Equations (24) and (25) can then be written as

$$\Sigma_j \left(\bar{D} + (j-\tfrac{1}{2})^2\pi^2 + \bar{l}^2\right)\Theta_j \sin(j-\tfrac{1}{2})\pi\zeta = -B_0\bar{w} \tag{A2}$$

$$\left(\frac{\mathrm{d}^2}{\mathrm{d}\zeta^2} - (A_0+E_0)\frac{\mathrm{d}}{\mathrm{d}\zeta} - \frac{\mathrm{d}A_0}{\mathrm{d}\zeta} + A_0E_0 - \bar{l}^2\right) \times \bar{w} = R_a\bar{l}^2F_0\Sigma_j\Theta_j \sin\left(j-\frac{1}{2}\right)\pi\zeta. \tag{A3}$$

Now if we insert the form

$$\bar{w} = R_a\bar{l}^2\Sigma_k\Theta_k W_k(\zeta) \tag{A4}$$

into equation (A3), we have

$$\left(\frac{\mathrm{d}^2}{\mathrm{d}\zeta^2} - (A_0+E_0)\frac{\mathrm{d}}{\mathrm{d}\zeta} - \frac{\mathrm{d}A_0}{\mathrm{d}\zeta} + A_0E_0 - \bar{l}^2\right) \times W_k = F_0 \sin\left(k-\frac{1}{2}\right)\pi\zeta \tag{A5}$$

which is required to satisfy the boundary condition (according to equations (A4) and (27)).

$$\frac{\mathrm{d}W_k}{\mathrm{d}\zeta}|_{\zeta=0} = 0, \quad W_k|_{\zeta=1} = 0. \tag{A6}$$

Equation (A5) is a second-order ordinary differential equation with variable coefficients. To solve this equation, we first make the following transformation

$$W_k = \mathrm{e}^{1/2\int_0^\zeta (A_0+E_0)\mathrm{d}\zeta} V_k \tag{A7}$$

we then have

$$\frac{\mathrm{d}W_k}{\mathrm{d}\zeta} = \frac{1}{2}(A_0+E_0)W_k + \mathrm{e}^{1/2\int_0^\zeta (A_0+E_0)\mathrm{d}\zeta}\frac{\mathrm{d}V_k}{\mathrm{d}\zeta}$$

$$\frac{\mathrm{d}^2W_k}{\mathrm{d}\zeta^2} = \mathrm{e}^{1/2\int_0^\zeta (A_0+E_0)\mathrm{d}\zeta}\left[\frac{1}{4}(A_0+E_0)^2V_k + \frac{V_k}{2}\frac{\mathrm{d}}{\mathrm{d}\zeta}(A_0+E_0) + (A_0+E_0)\frac{\mathrm{d}V_k}{\mathrm{d}\zeta} + \frac{\mathrm{d}^2V_k}{\mathrm{d}\zeta^2}\right]. \tag{A8}$$

Substitution of equation (A8) into (A5) gives

$$\frac{\mathrm{d}^2V_k}{\mathrm{d}\zeta^2} - \frac{V_k}{2}\frac{\mathrm{d}}{\mathrm{d}\zeta}(A_0-E_0) - \frac{1}{4}(A_0-E_0)^2V_k - \bar{l}^2V_k = (F_0 \sin\left(k-\frac{1}{2}\right)\pi\zeta)\,\mathrm{e}^{-1/2\int_0^\zeta (A_0+E_0)\mathrm{d}\zeta} \tag{A9}$$

with boundary condition (A6) becomes

$$\frac{\mathrm{d}V_k}{\mathrm{d}\zeta} + \frac{1}{2}(A_0+E_0)V_k|_{\zeta=0} = 0; \quad V_k|_{\zeta=1} = 0. \tag{A10}$$

To solve equation (A9) for V_k, we employ WKB method [39, p. 27], which gives

$$V_k = \frac{1}{f^{1/4}}(c_1(\zeta)\,\mathrm{e}^{\int_0^\zeta \sqrt{f}\mathrm{d}\zeta} + c_2(\zeta)\,\mathrm{e}^{-\int_0^\zeta \sqrt{f}\mathrm{d}\zeta})$$

$$f = \frac{1}{2}\frac{\mathrm{d}}{\mathrm{d}\zeta}(A_0-E_0) + \frac{(A_0-E_0)^2}{4} + \bar{l}^2$$

$$c_1(\zeta) = c_1^0 + \frac{1}{2}\int_0^\zeta f^{-1/4} \times \exp\left(-\int_0^\zeta \sqrt{f}\mathrm{d}\zeta - \frac{1}{2}\int_0^\zeta A_0\,\mathrm{d}\zeta\right)F_0 \sin\left(k-\frac{1}{2}\right)\pi\zeta\,\mathrm{d}\zeta$$

$$c_2(\zeta) = c_2^0 - \frac{1}{2}\int_0^\zeta f^{-1/4} \times \exp\left(\int_0^\zeta \sqrt{f}\,\mathrm{d}\zeta - \frac{1}{2}\int_0^\zeta A_0\,\mathrm{d}\zeta\right) F_0 \sin\left(k-\frac{1}{2}\right)\pi\zeta\,\mathrm{d}\zeta. \quad \text{(A11)}$$

The integral constants c_1^0 and c_2^0 can be determined by the boundary conditions (A10), i.e.

$$c_1^0 = \frac{1+\dfrac{A_0(0)+E_0(0)}{2f^{1/2}(0)}}{1-\dfrac{A_0(0)+E_0(0)}{2f^{1/2}(0)}}c_2^0$$

$$c_1^0 = \frac{1}{2}\mathrm{e}^{-\int_0^1\sqrt{f}\,\mathrm{d}\zeta}\int_0^1 f^{1/4} \times \exp\left[\int_0^\zeta \sqrt{f}\,\mathrm{d}\zeta - \frac{1}{2}\int_0^\zeta (A_0+E_0)\,\mathrm{d}\zeta\right] F_0 \sin\left(k-\frac{1}{2}\right)\pi\zeta\,\mathrm{d}\zeta - \frac{1}{2}\mathrm{e}^{\int_0^1\sqrt{f}\,\mathrm{d}\zeta}\int_0^1 f^{1/4} \times \exp\left[-\int_0^\zeta \sqrt{f}\,\mathrm{d}\zeta - \frac{1}{2}\int_0^\zeta (A_0+E_0)\,\mathrm{d}\zeta\right] F_0 \sin\left(k-\frac{1}{2}\right)\pi\zeta\,\mathrm{d}\zeta \left[\mathrm{e}^{\int_0^1\sqrt{f}\,\mathrm{d}\zeta} + \frac{2\sqrt{f}(0)+A_0(0)+E_0(0)}{2\sqrt{f}(0)-A_0(0)+E_0(0)}\mathrm{e}^{-\int_0^1\sqrt{f}\,\mathrm{d}\zeta}\right]^{-1}. \quad \text{(A12)}$$

To solve Θ_k, we substitute equation (A4) into equation (A2) and obtain

$$\Sigma_j(\bar{D}+j^2\pi^2+\bar{l}^2)\Theta_j \sin(j-\tfrac{1}{2})\pi\zeta = -B_0 Ra\bar{l}^2\,\Sigma_k\Theta_k V_k. \quad \text{(A13)}$$

From the theory of the Fourier sine series transform, we have

$$B_0 W_k = \Sigma_j\left(z\int_0^1 B_0 W_k \sin\left(j-\frac{1}{2}\right)\pi\zeta\,\mathrm{d}\zeta\right)\sin\left(j-\frac{1}{2}\right)\pi\zeta. \quad \text{(A14)}$$

Substituting the above equation into equation (A13) gives

$$\Sigma_j(\bar{D}+j^2\pi^2+\bar{l}^2)\Theta_j \sin(j-\tfrac{1}{2})\pi\zeta + 2Ra\bar{l}^2\,\Sigma_k\Sigma_j\Theta_k\left(\int_0^1 B_0 W_k \sin\left(j-\frac{1}{2}\right)\pi\zeta\,\mathrm{d}\zeta\right) \times \sin\left(j-\frac{1}{2}\right)\pi\zeta = 0. \quad \text{(A15)}$$

Because each term must vanish individually, the above equation can also be written as

$$\sum_{k=0}^{\infty}\Pi_{jk}\Theta_k = 0$$

$$\Pi_{jk} = (\bar{D}+j^2\pi^2+\bar{l}^2)\delta_{jk} + 2R_a\bar{l}^2\int_0^1 B_0 W_k \sin\left(j-\frac{1}{2}\right)\pi\zeta\,\mathrm{d}\zeta. \quad \text{(A16)}$$